Non-Newtonian Viscosity of *Escherichia coli* Suspensions

Jérémie Gachelin, Gastón Miño, Hélène Berthet, Anke Lindner,* Annie Rousselet, and Éric Clément
PMMH-ESPCI, UMR 7636 CNRS-ESPCI-Universities Pierre et Marie Curie and Denis Diderot, 10 rue Vauquelin, 75005 Paris, France
(Received 5 October 2012; published 26 June 2013)

The viscosity of an active suspension of *E. coli* bacteria is determined experimentally as a function of the shear rate using a Y-shaped microfluidic channel. From the relative suspension viscosity, we identify rheological thickening and thinning regimes as well as situations at low shear rate where the viscosity of the bacteria suspension can be lower than the viscosity of the suspending fluid. In addition, bacteria concentration and velocity profiles in the bulk are directly measured in the microchannel.

DOI: 10.1103/PhysRevLett.110.268103 PACS numbers: 47.63.−b, 47.57.Qk, 47.57.E−

The fluid mechanics of microscopic swimmers in suspension have been widely studied in recent years. Bacteria [1,2], algae [3,4], or artificial swimmers [5] dispersed in a fluid display properties that differ strongly from those of passive suspensions [6]. The physical relationships governing momentum and energy transfer as well as constitutive equations vary drastically for these suspensions [7,8]. Unique physical phenomena caused by the activity of swimmers were recently identified such as enhanced Brownian diffusivity [1,8–10], uncommon viscosity [4,11,12], active transport and mixing [13], or the extraction of work from chaotic motion of bacteria [12,14]. The presence of living and cooperative species may also induce collective motion and organization at the mesoscopic or macroscopic level [15,16], impacting the constitutive relationships in the semi-dilute or dense regimes.

The *E. coli* bacterium (typical length $D = 2\ \mu$m) possesses a quite sophisticated propulsion apparatus consisting of a collection of flagella (7–10 μm length) organized in a bundle attached at the rear of the bacterium and rotating counterclockwise [17]. It has the ability to change direction (a tumble) at a given frequency by unbundling its flagella [18]. In spite of the inherent complexity of the propulsion features, low Reynolds number hydrodynamics impose a long range flow field which can be modeled as an effective force dipole. Due to the thrust coming from the rear, *E. coli* are described as "pushers," hence defining a sign for the force dipole which has a crucial importance on the rheology of active suspensions [7]. For a dilute suspension of force dipoles, Haines *et al.* [19] and Saintillan [20] derived an explicit relation relating viscosity and shear rate. They obtained an effective viscosity similar in form to the classical Einstein relation for dilute suspensionsusing the space occupied by the body: $\eta = \eta_0(1 + K\phi)$ (η_0 is the suspending fluid viscosity and ϕ the volume fraction). These theories predict a negative value for the coefficient K for pushers at low shear rates, meaning the suspension can exhibit a lower viscosity than the suspending fluid. The theoretical assessment of shear viscosity relies on an assumed statistical representation of the orientations of the bacteria, captured by a Fokker-Plank equation and a kinematic model for the swimming trajectories [21,22].

Despite the large number of theoretical studies, few experiments have been conducted. With *Bacillus subtilis* (pushers) trapped in a liquid film, Sokolov *et al.* [11] have shown that a vorticity decay rate could be associated with a strong decrease of shear viscosity in the presence of bacteria. For algae (pullers), Rafai *et al.* [4] have shown that the effective viscosity measured in a classical rheometer is larger than the viscosity of the corresponding dead (passive) suspension. However, no measurements of the viscosity of a dilute suspension of pushers under controlled shear conditions exist to date. This is mainly due to the fact that one has to assess low viscosities near the viscosity of water at very low shear rates to probe the theoretical predictions. These parameters are typically outside of the resolution of a classical rotational rheometer and have thus made these measurements inaccessible. In this letter, we present the first measurements of the shear viscosity of a suspension of pushers using a microfluidic device to overcome these difficulties and obtain the relative viscosity of an active suspension for a large range of shear rates and bacteria concentrations. Our setup also allows direct visualization of the flow as well as the spatial distributions of bacteria in the flow.

The wild type *E. coli* W used here are prepared following the experimental procedures described in Refs. [9,23]. The strain is grown overnight in rich medium (LB). After washing, it is transferred into MMA, a motility medium supplemented with K-acetate (0.34 mM) and polyvinyl pyrolidone (PVP: 0.005%). The sample is then incubated for at least one hour. To avoid bacteria sedimentation, Percoll is mixed with MMAP 1 vol/1 vol (isodense conditions). The suspending fluid is Newtonian with viscosity $\eta = 1.28 \times 10^{-3}$ Pa s at 22 °C. All experiments are performed at a fixed temperature $T = 25$ °C. In a fluid at rest our bacteria swim at an average speed of $U = 20\ \mu$m/s and tumble at a typical frequency of 1 Hz. To gain unambiguous information on the role of bacteria activity we have also worked with nonmotile bacteria,

changing the bacteria morphology as little as possible. The bacteria are asphyxiated with Sodium Azide and kept at $T = 4\,^{\circ}\mathrm{C}$ overnight. Observation under a microscope of the bacteria within a fluid at rest confirmed the nonmotility. Note however that it is likely that the flagella unbundle if the bacterium does not swim, changing the morphology of nonmotile bacteria compared to their motile counterparts.

To obtain the shear viscosity, we adapted a microfluidic device [24] comparing the Newtonian viscosities of two liquids. The device is a Y-shaped Hele-Shaw cell of height h, such that each branch receives a different fluid, respectively fluid 0 of viscosity η_0 and fluid 1 of viscosity η_1 (see Fig. 1). Both flows are driven at an identical flow rate Q. In a Hele-Shaw approximation, the dominant shear rate occurs in the direction of the cell height z. In addition, for a viscosity ratio close to one, the velocities of the two fluids in the main channel differ only slightly and the shear occurring at the interface of the two fluids in the x direction can be neglected compared to the shear in the z direction. Under these conditions, at steady state the viscosity ratio η_1/η_0 can be directly obtained from the position of the interface between both fluids d_1/d_0 [24]. Guillot *et al.* [24] have also used this approach for non-Newtonian fluids, where it corresponds to the measurement of an apparent viscosity. Here we will follow the same approach and will verify our method subsequently. The suspension of bacteria is flowed into one arm and the suspending Newtonian fluid into the other arm. The interface position is then measured at various flow rates Q. The experimental data is presented as a function of the maximum shear rate obtained by assuming a parabolic flow profile in the channel height $\dot{\gamma}_M = (6Q)/(h^2 d_1)$, where d_1 is the lateral width occupied by the suspension. The relative viscosity $\eta_r =$ is then

$$\eta_r = \frac{\eta_1}{\eta_0} = \frac{d_1}{d_0}. \tag{1}$$

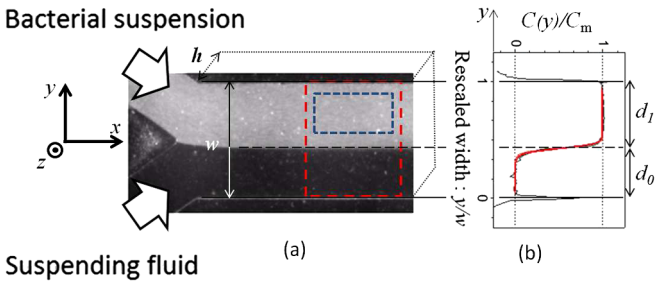

FIG. 1 (color online). Experimental setup. (a) Time-averaged image of the microchannel ($W = 600\ \mu$m) for $Q = 10$ nl/sec in each branch and volume fraction $\phi = 0.35\%$. Bacteria are visualized using a white light microscope. The red and blue frames indicate the measurement areas. (b) Concentration profile $C(y)$ normalized by the maximum concentration C_M (black line) and error function fit used to determine the interface position (red line).

This microfluidic device has the advantage of measuring a viscosity ratio and provides very good resolution of the suspension viscosity independent of its absolute value or the applied shear rate. We use a very high precision two-syringe pump from nemeSYS and a precision syringe (Hamilton Gastight 1805RN) of a very small volume (50 μl) allowing us to impose identical and very small flow rates (down to $Q = 0.5$ nl/sec) on both arms. Test experiments with passive suspensions formed by PS beads (micromod, diameter 2 μm) at small volume fractions ($\phi = 1$–10%) have been carried out and show that our device can measure relative viscosities for these concentrations with high precision.

The Y-shaped channel was fabricated completely from PDMS using a soft-lithography technique. The channel thickness is $h = 100\ \mu$m. The main channel width is $w = 600\ \mu$m and the two inlet branch widths are $w/2$. Inlets are connected by 500 μm diameter tubes to the two-syringe pump. The total length of the main channel is 40 mm. Suspensions were prepared (see [9]) with a number of bacteria per unit volume n in the range $1.9 \times 10^{12}\ 1^{-1} < n < 25.6 \times 10^{12}\ 1^{-1}$. The concentration of bacteria is determined by measuring the optical density of the suspension and using a calibration curve. The volume fraction is estimated using the space occupied by the body of each bacteria $v_b = 1\ \mu\mathrm{m}^3$ such that $\phi = n v_b$, yielding a range of $0.19 < \phi < 2.56\%$. The flowing suspension was observed using an inverted microscope (Zeiss-Observer, Z1) connected to a digital camera (PixeLINK PL-A741-E, 1280×1024 pix^2) capturing videos at a frame rate of 22 images/s using white light. Low magnification $2.5\times$ allowed an extended view of the channel (see Fig. 1). The interface reaches its equilibrium position at approximately 600 μm from the junction of the two inlet channels and this position is then stable over the whole length of the channel. A widening of the interface is observed further downstream from the inlet due to "active" diffusion of the swimming bacteria. We have chosen the sample region (indicated by the red rectangle on Fig. 1) in such a way as to be in steady state conditions while avoiding significant widening of the interface.

During an experiment we increase the flow rate step by step from $Q = 0.5$ nl/sec to $Q = 100$ nl/sec. Note that we have verified for all experiments that identical results are obtained when subsequently decreasing the flow rate. In Fig. 1, the shape of the interface obtained by averaging over 120 successive images is displayed for the measurement area. To quantitatively determine the interface position, we measure the mean light intensity $\langle I\rangle(y)$ across the channel width averaging in the x direction over a distance of 600 μm (see red rectangle in Fig. 1). $C(y) = \ln(\langle I\rangle(y)/\langle I\rangle_0)$, with $\langle I\rangle_0$ being the mean intensity in the absence of bacteria, is then fitted with an error function $\mathrm{erf}(y)$ to obtain the interface position y_I. Once the interface position is determined, we extract the relative viscosity [Eq. (1)] and associate it with $\dot{\gamma}_M$.

Experimental observations are presented in the inset of Fig. 2(a) displaying averaged images for flow rates of $Q = 0.5$ nl/sec, $Q = 2$ nl/sec, and $Q = 10$ nl/sec for a suspension at a volume fraction of $\phi = 0.35\%$. When increasing the flow rate the interface position changes from a value above the midposition to a value below the midposition indicating a change in the suspension viscosity from lower than the viscosity of the suspending fluid to greater.

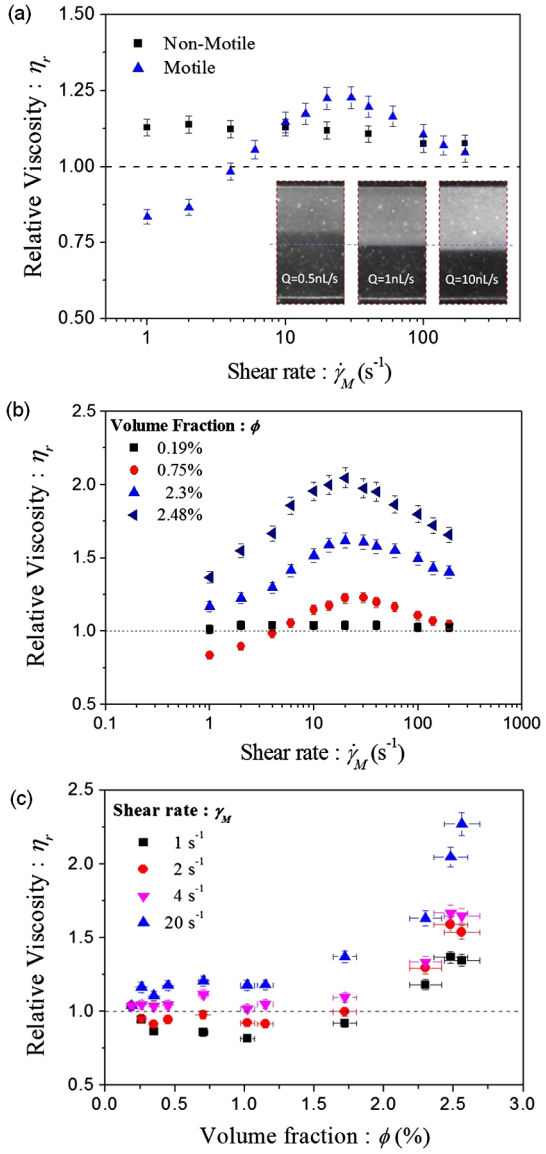

FIG. 2 (color online). Rheology curves. (a) Relative viscosity versus maximum shear rate for motile and nonmotile bacteria at $\phi = 0.8\%$. Inset: Three averaged pictures of the bilaminar flow for flow rates of $Q = 0.5$ nl/s, $Q = 2$ nl/s, and $Q = 10$ nl/s, respectively, for a $\phi = 0.35\%$ bacteria suspension. These images are averaged over 120 images at 22im/s and observed with a 2.5× magnification using phase contrast. The dotted line represents the center position in the channel width. The scale bar corresponds to 200 μm. (b) η_r versus $\dot{\gamma}_M$ at several volume fractions (c) η_r versus ϕ at several shear rates. The errors bars are estimated using the detection error of the interface position.

Quantitative measurements are given in Fig. 2(a) showing the relative viscosity η_r of suspensions of motile and nonmotile bacteria as a function of the maximum shear rate for a concentration of $\phi = 0.8\%$. For the motile bacteria we observe a relative viscosity below one at small shear rates, an increase of viscosity with increasing shear rate (shear thickening) and then shear thinning occurs at higher shear rates. The maximum viscosity is observed at a value of approximately $\dot{\gamma}_M = 20$ s^{-1}. This nonmonotonic behavior as a function of shear rate is in agreement with the results of Saintillan [20] obtained for slender bacteria and can be explained as follows. For shear rates smaller than the inverse of a typical time of bacteria swimming, normally taken as the ratio between the swimming speed and the length of the bacterium U/D, bacteria activity is dominant and the viscosity is decreased. For shear rates larger than this value the activity of the bacteria becomes negligible compared to the effect of the shear flow and the behavior of a passive suspension of rods is recovered. In our case $U/D \sim 10$ s^{-1} is indeed comparable to $\dot{\gamma}_M = 20$ s^{-1}. The viscosity of the nonmotile bacteria does not show a decrease in viscosity below one or shear thickening behavior. This nonmonotonic behavior is thus undoubtedly due to bacteria activity. For shear rates larger than $\dot{\gamma}_M = 20$ s^{-1} the behavior of the two curves becomes similar and is comparable to a passive suspension of rods. Results for different concentrations are given in Fig. 2(b) showing the relative viscosity η_r as a function of the maximum shear rate for various concentrations $\phi = 0.2\%$, 0.8%, 2.3%, and 2.5%. Note that for the lowest concentration the viscosity of the Newtonian suspending fluid is recovered for all shear rates validating again our rheological device. For all other concentrations, the curves display the same qualitative behavior as shown on Fig. 2(a) and the maximum in viscosity occurs at the same shear rate for all concentrations. For all of these cases, the shear thinning and shear thickening character of the active suspensions are weak and power law indices n (using $\eta = K\dot{\gamma}^{(n-1)}$) close to one are found for both regimes for all concentrations. Figure 2(c) shows the relative viscosity as a function of the volume fraction ϕ at various shear rates $\dot{\gamma}_M = 1$, 2, 4, and 20 s^{-1}. A decrease in viscosity below one is observed for the small shear rates, confirming in this way the theoretical predictions [19,20]. With increasing concentration a sharp increase of viscosity takes place for all shear rates, corresponding to a semi-dilute regime. In our case this regime is observed for concentrations above approximately 1%. Similar behavior was also observed by Sokolov *et al.* [11] using vortex decay in a suspension of *Bacilus subtilis* in a liquid film and has been predicted by Ryan *et al.* [25] in their simulations.

One of the advantages of our microfluidic device is that we can directly access the local velocity and bacteria concentration profiles as a function of the channel height. Bacteria moving in the flow were visualized with a high

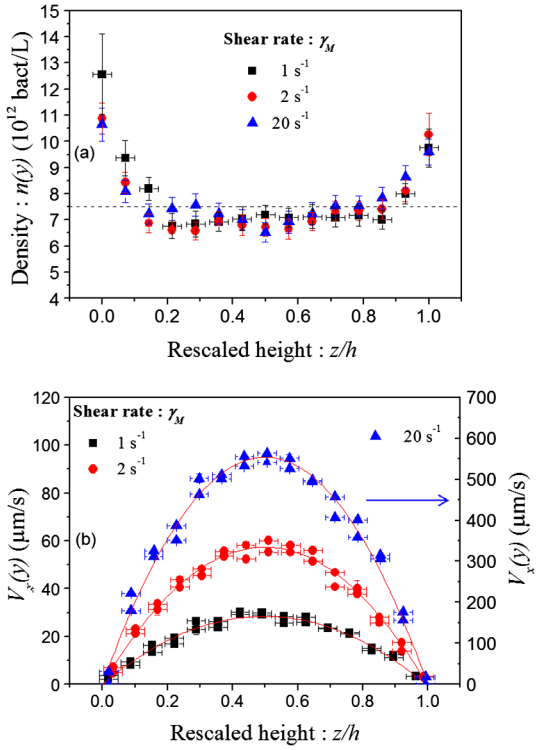

FIG. 3 (color online). Bulk profile measurements for a volume fraction $\phi = 0.75\%$ and shear rates $\dot{\gamma}_M = 1,\ 2,\ 20\ \mathrm{s}^{-1}$. (a) Bacteria density profile $n(z)$. The horizontal dashed line represents the mean density: $\bar{n} = 7.5 \times 10^{12}$ bact/l. (b) Velocity profile of passive tracers $V_x(z)$.

magnification objective (40x, phase contrast) allowing the position of the bacteria to be monitored at various heights z (field depth 3 μm). Videos were taken using a high-speed camera (Photron FastCam SA3, resolution 1024×1024 pixels, shutter speed (1/500 s), frame rate 1/50 s for $Q = 0.5$, 1nl/s and 1/500 s for $Q = 10$ nl/s). To monitor the flow velocity, we suspended a very low concentration of 2 μm density-matched latex beads as passive tracers (density 1.03 g/cm^3). Here we present selected results for the volume fraction $\phi = 0.75\%$ at which the reduction of the relative viscosity below 1 is observed at three flow rates ($Q = 0.5$, 1, 10 nl/ sec corresponding respectively to maximum shear rates $\dot{\gamma}_M = 1$, 2, 20 s^{-1}. Videos were taken in a region centered between the interface and the side wall (see blue frame of Fig. 1). To reduce the detection noise, a bacterium is retained only if it is detected on at least two consecutive frames. The flow velocities were computed for particles moving in the focal plane. In Fig. 3(a) we see that the concentration profiles are similar in shape to those published previously by [23] in the absence of flow, i.e., a quasiconstant density and a strong density increase within 10 μm of the wall, hence probing a trapping effect that persists over the range of shear rates explored. The calculated mean concentration is represented by the dashed line in Fig. 3(a) and is in agreement with the measured bulk concentration. It is important to note that the concentration profiles are identical for the various shear rates. The change in viscosity observed is therefore not due to a change in concentration within the microchannel. The velocity profiles $V_x(z)$ are displayed in Fig. 3(b). Within the precision of our experimental setup, a deviation from a parabolic velocity profile is not observed justifying the approximation used for our analysis. Note also that this finding is in agreement with the weak shear thinning or shear thickening character of our suspensions, for which only small changes in the velocity profile are predicted and not detectable in our experiments.

In conclusion, using a microfluidic device, we have measured for the first time the effective viscosity of a suspension of "pushers" (*E. coli* bacteria) as a function of the shear rate over a large range (1–200 s^{-1}) in the dilute and semi-dilute regimes. We confirmed in this way an important prediction for the rheology of pushers: at small shear rates the active viscosity can be smaller then the viscosity of the suspending fluid [7,19,20]. In the dilute as well as in the semi-dilute regime, we observed a shear-thickening behavior at lower shear rates followed by a shear-thinning regime at higher shear rates. The viscosity maximum is observed at a shear rate on the order of the inverse of the time a bacterium needs to swim over a distance of its own length and this value seems independent of the bacteria concentration. These results are consistent with the theoretical calculations of Saintillan [20] conducted in the dilute regime for a simple shear flow using a slender-body (rodlike) representation for the swimmer shape. In the semi-dilute regime (here for volume fractions greater than 1%), we observe a strong increase of the viscosity consistent with numerical simulations by Ryan *et al.* [25]. Our results represent the first experimental validation of the non-Newtonian rheology of an active suspension of pushers under controlled shear conditions. These results are an important experimental validation of the consequences of the original hydrodynamics of active particle systems, and will serve as a validation for the large number of theoretical and numerical studies in this field. In a larger context these results are important for the understanding of bacteria transport, in biomedical applications, biofuel production or soil decontamination.

G. M. acknowledges financial support of the Pierre-Gilles de Gennes Foundation and a MRES special grant. We thank Professors R. Soto, D. Saintillan, I. Aronson, and M. Alves for enlightening scientific discussions and C. Davis for a careful reading of the manuscript.

*anke.lindner@espci.fr

[1] X.-L. Wu and A. Libchaber, Phys. Rev. Lett. **84**, 3017 (2000).

[2] C. Dombrowski, L. Cisneros, S. Chatkaew, R. E. Goldstein, and J. O. Kessler, Phys. Rev. Lett. **93**, 098103 (2004).

[3] K. C. Leptos, J. S. Guasto, J. P. Gollub, A. I. Pesci, and R. E. Goldstein, Phys. Rev. Lett. **103**, 198103 (2009).
[4] S. Rafaï, L. Jibuti, and P. Peyla, Phys. Rev. Lett. **104**, 098102 (2010).
[5] W. F. Paxton, K. C. Kistler, C. C. Olmeda, A. Sen, S. K. St. Angelo, Y. Cao, T. E. Mallouk, P. E. Lammert, and V. H. Crespi, J. Am. Chem. Soc. **126**, 13 424 (2004).
[6] A. Baskaran and M. C. Marchetti, Proc. Natl. Acad. Sci. U.S.A. **106**, 15 567 (2009); D. L. Koch and G. Subramanian, Annu. Rev. Fluid Mech. **43**, 637 (2011).
[7] Y. Hatwalne, S. Ramaswamy, M. Rao, and R. A. Simha, Phys. Rev. Lett. **92**, 118101 (2004).
[8] D. T. N. Chen, A. Lau, L. Hough, M. Islam, M. Goulian, T. Lubensky, and A. Yodh, Phys. Rev. Lett. **99**, 148302 (2007).
[9] G. Mino, T. E. Mallouk, T. Darnige, M. Hoyos, J. Dauchet, J. Dunstan, R. Soto, Y. Wang, A. Rousselet, and E. Clement, Phys. Rev. Lett. **106**, 048102 (2011).
[10] P. T. Underhill, J. P. Hernandez-Ortiz, and M. D. Graham, Phys. Rev. Lett. **100**, 248101 (2008).
[11] A. Sokolov and I. S. Aranson, Phys. Rev. Lett. **103**, 148101 (2009).
[12] R. Di Leonardo, L. Angelani, D. Dell'Arciprete, G. Ruocco, V. Iebba, S. Schippa, M. P. Conte, F. Mecarini, F. De Angelis, and E. Di Fabrizio, Proc. Natl. Acad. Sci. U.S.A. **107**, 9541 (2010).
[13] M. J. Kim and K. S. Breuer, Anal. Chem. **79**, 955 (2007).
[14] A. Sokolov, M. M. Apodaca, B. A. Grzybowski, and I. S. Aranson, Proc. Natl. Acad. Sci. U.S.A. **107**, 969 (2010).
[15] G. Gregoire, H. Chate, and Y. Tu, Phys. Rev. E **64**, 011902 (2001).
[16] D. Saintillan and M. J. Shelley, J. R. Soc. Interface **9**, 571 (2012).
[17] H. C. Berg, *E. coli in Motion* (Verlag, New York, 2004).
[18] N. C. Darnton, L. Turner, S. Rojevsky, and H. C. Berg, J. Bacteriol. **189**, 1756 (2007).
[19] B. M. Haines, A. Sokolov, I. Aranson, L. Berlyand, and D. Karpeev, Phys. Rev. E **80**, 041922 (2009)
[20] D. Saintillan, Exp. Mech. **50**, 1275 (2010).
[21] F. P. Bretherton, J. Fluid Mech. **14**, 284 (1962); G. B. Jeffery, Proc. R. Soc. A **102**, 161 (1922).
[22] A. Zöttl and H. Stark, Phys. Rev. Lett. **108**, 218104 (2012).
[23] A. P. Berke, L. Turner, H. C. Berg, and E. Lauga, Phys. Rev. Lett. **101**, 038102 (2008).
[24] P. Guillot, P. Panizza, J.-B. Salmon, M. Joanicot, A. Colin, C.-H. Bruneau, and T. Colin, Langmuir **22**, 6438 (2006); P. Galambos and F. Forster, *Micro-Electro-Mechanicical System (MEMS), 1998* p. 187 (unpublished); P. Nghe, P. Tabeling, and A. Ajdari, J. Non-Newtonian Fluid Mech. **165**, 313 (2010).
[25] S. Ryan, B. M. Haines, L. Berlyand, F. Ziebert, and I. S. Aranson, Phys. Rev. E **83**, 050904 (2011).